THE ASTROPHYSICAL JOURNAL, 400:214–221, 1992 November 20

SPECTROSCOPY OF A BALMER-DOMINATED FILAMENT IN THE CYGNUS LOOP WITH THE HOPKINS ULTRAVIOLET TELESCOPE

KNOX S. LONG
Space Telescope Science Institute, 3700 San Martin Drive, Baltimore, MD 21218

WILLIAM P. BLAIR, OLAF VANCURA, CHARLES W. BOWERS, AND ARTHUR F. DAVIDSEN
Center for Astrophysical Sciences, Department of Physics and Astronomy, The Johns Hopkins University, Charles & 34th Streets, Baltimore, MD 21218

AND

JOHN C. RAYMOND
Smithsonian Astrophysical Observatory, 60 Garden Street, Cambridge, MA 02138
Received 1992 February 7; accepted 1992 May 29

ABSTRACT

We have obtained a fair ultraviolet spectrum of a nonradiative filament in the Cygnus Loop covering the wavelength range 830–1860 Å at 3.5 Å resolution using the Hopkins Ultraviolet Telescope on the *Astro-1* space shuttle mission. The spectrum shows strong emission lines of high-ionization species, including O VI $\lambda\lambda$1032, 1038, N V $\lambda\lambda$1239, 1243, O V λ1371, C IV $\lambda\lambda$1548, 1551, and He II λ1640, as well as fainter lines never before seen in nonradiative shock spectra. The O VI doublet is of particular interest because it comes from a hotter region in the postshock flow than other UV lines and because the doublet ratio can be used to assess the amount of resonant line scattering at this position. We calculate nonradiative shock models which include a more sophisticated treatment of Lyman line transfer. We find that the HUT spectrum can be explained in terms of a shock with velocity 175–185 km s^{-1} propagating into a low-density medium. This shock velocity can be reconciled with the $\sim$135 km s^{-1} width of the broad component of Hα in this filament if equilibration of the postshock electron and ion temperatures proceeds much more rapidly than Coulomb equilibration timescales. However, the time required for a 180 km s^{-1} shock to develop a partial recombination zone is short, $\sim$200 yr if $n \sim 2$ cm^{-3}. This suggests that the shock is decelerating as it encounters denser material. Therefore, we have also developed a simple model in which the shock has decelerated rapidly from $\sim$200 km s^{-1} to $\sim$130 km s^{-1}. This model can match the Hα line width and the O VI:N V line ratio assuming that only Coulomb collisions transfer energy from ions to electrons, but it does not match the rest of the HUT spectrum as well as a single velocity and rapid equilibration. Although more sophisticated modeling is needed, the current analysis clearly favors rapid equilibration of electrons and ions behind the shock.

Subject headings: ISM: individual (Cygnus Loop) — shock waves — supernova remnants — ultraviolet: interstellar

1. INTRODUCTION

The Cygnus Loop has a limb brightened morphology at X-ray, optical, infrared, and radio wavelengths (Ku et al. 1984; Braun & Strom 1986; Keen et al. 1973). It lies along a line of sight with very little interstellar absorption [$E(B-V) = 0.08$; Miller 1974; Fesen, Blair, & Kirshner 1982]. At an assumed distance of 770 kpc (Fesen et al. 1982; Hester, Raymond, & Danielson 1986) its angular size, $\sim 3° \times 3.^\circ 7$, corresponds to linear dimensions of 40 × 50 pc. X-ray observations suggests that the primary SN shock in the Cygnus Loop is expanding with a velocity of $\sim$400 km s^{-1} into an interstellar medium (ISM) with a mean density of $\sim$0.2 cm^{-3} and that the age of the Cygnus Loop is of order 18,000 yr (Ku et al. 1984). There is clear evidence that the primary shock has also encountered clouds with preshock densities of 10–30 cm^{-3}; secondary shocks, driven into and through these clouds with velocities of 100–200 km s^{-1}, produce the bright optical/UV emission observed over roughly one-third of the periphery of the SNR (Raymond et al. 1980, 1981; Benvenuti, Dopita, & D'Odorico 1980; Fesen et al. 1982; Blair et al. 1991b). The Cygnus Loop is probably nearing the end of the adiabatic phase or just entering the radiative phase of its evolution. Because of the proximity, large angular size, relatively low extinction, and brightness of the Cygnus Loop, individual filaments can be studied in great detail. As a result, the Cygnus Loop provides some of the most exactly confrontations of observational fact with the theory of shocks in a multiphase ISM (see, e.g. Raymond et al. 1988).

The optical spectra of the bright filaments in the Cygnus Loop show forbidden lines such as [O III], [N II], and [S II] that are comparable in strength to Hα. However, there exists an extensive series of filaments along the northern rim of the remnant in which the Balmer lines of hydrogen are present but the forbidden lines are weak or entirely absent (Raymond et al. 1983, hereafter RBFG; Fesen & Itoh 1985; Hester, Raymond, & Danielson 1986). Unlike the bright optical filaments, which are mainly located interior to the supernova shock front as delineated by X-ray maps of the Cygnus Loop, these Balmer-dominated shocks appear to be closely associated with the main blast wave of the SN explosion. The spectra from these Balmer-dominated filaments are usually interpreted in terms of a fast shock in a low-density, partially neutral medium (Chevalier & Raymond 1978; McKee & Hollenbach 1980; Chevalier, Kirschner, & Raymond 1980, hereafter CKR). Permitted lines dominated the emission in the ionizing plasma; a recombination zone (which would produce copious forbidden-

line emission) does not exist for these shocks, since the cooling time behind the fast shock in a low-density medium is long.[1] Such shocks are also called nonradiative shocks because the structure of the shock is not strongly modified by radiative cooling. In addition to those in the Cygnus Loop, Balmer-dominated filaments have been identified in a number of (mostly young) SNRs: SN 1006 (Schweizer & Lasker 1978; Long, Blair, & van den Bergh 1988), Tycho's SNR (Kirshner & Chevalier 1978; Kirschner, Winkler, & Chevalier 1987), Kepler's SNR (Fesen et al. 1989; Blair, Long, & Vancura 1991), RCW86 (Long & Blair 1990) and four SNRs in the Large Magellanic Cloud (Tuohy et al. 1982; Smith et al. 1991).

Because of the close connection of these Balmer-dominated shocks with the primary shock front of an SNR, it is important to obtain a better understanding of these relatively rare (or at least rarely observed) shocks. Ultraviolet observations are particularly important because of the rich spectrum of permitted lines in this wavelength range and because the strengths of the high-ionization permitted lines are strongly affected by the velocity of the shock and the state of the plasma, specifically the postshock electron temperature. We have observed a relatively bright Balmer-dominated filament in the northeast Cygnus Loop with the Hopkins Ultraviolet Telescope as part of the *Astro-1* shuttle mission in 1990 December. This was one of two observations of the Cygnus Loop made with HUT; the other observation, measuring the far UV emission of a shock with an extant, but incomplete, recombination zone, has been described by Blair *et al.* (1991a). The Balmer-dominated filament discussed here has been observed by RBFG with the *International Ultraviolet Explorer* (*IUE*); aside from the nearby filament studied by Hester et al. (1992), it is the only Balmer-dominated filament which has ever been observed successfully in the UV. RBFG found they could explain the UV and optical spectrum of this filament with a shock velocity of 170 km s^{-1} if postshock electron-ion equilibration occurred primarily through Coulomb interactions. This paper reports the first observation to clearly resolve the spectral features of a Balmer-dominated filament in the sub-Lyα range, which includes O VI $\lambda\lambda$1032, 1038.

2. OBSERVATIONS

The Hopkins Ultraviolet Telescope (HUT) has been described by Davidsen et al. (1992). The instrument includes a 0.9 m iridium-coated mirror that feeds a prime focus Rowland spectrograph. The spectrograph consists of a holographically generated osmium-coated concave grating which diffracts light entering one of eight selectable apertures onto a CsI-coated microchannel plate detector with a phosphor-coated image converter. A photodiode array detector, operated in a photon counting mode, is used to read out the spectrum. The instrument covers the wavelength range 830–1860 Å in first order.

The observation of the Balmer-dominated filament, which is located at $20^h53^m59^s$ and 31°45′06″ (1950), was carried out using the 9″.4 × 116″ slit at a position angle of 135°. The slit position is shown on a portion of an Hα image of the NE limb of the Cygnus Loop obtained with the KPNO 4 m telescope in Figure 1 (Plate 1). With this slit and an extended source, the spectral resolution is ~3.5 Å. The payload specialist positioned the aperture on the sky by matching predefined guide stars to a set of guide star fiducials placed on the acquisition TV screen by the dedicated experiment processor of the HUT instrument. Data were acquired for a total of 1730 s. However, the pointing was not very stable during the first two-thirds of the observations. Therefore, we have confined our analysis to a 670 s period at the end of the observation when the RMS pointing stability in the direction perpendicular to the slit was ~0″.9. Fortunately this portion of the observation took place during orbital night when airglow emissions are confined primarily to Lyα, Lyβ, O I λ1304, and O I λ1356. This on-target part of the observation was immediately preceded by a 240 s period in which the slit was located 15′ east of the filament and in which there is no evidence of emission from the Cygnus Loop. This off-target portion of the observation also took place in orbital night, as evidenced by the weakness of lines such as O II λ834, O I λ989, and N I λ1134, which are prominent in dayglow spectra obtained with HUT. We have used this off-target data to remove much of the residual airglow from the on-target observation of the nonradiative filament in the Cygnus Loop.

To obtain the source spectrum, we have first flux-calibrated the data obtained during the on-target and off-target portions of the observations separately. This process involves subtracting the dark counts and scattered light in the detector as estimated from an airglow-free region of the spectrum below the Lyman limit, making a modest correction for doubly-counted events, which arise due to phosphor persistence in the detector, and dividing the time-average count rate spectrum by the effective area of the telescope as determined by a combination of prelaunch and in-flight calibrations (see Davidsen et al. 1992). We then scaled and subtracted the airglow spectrum from the on-target spectrum. The airglow spectrum was scaled to match the strength of Lyα, which is ~45 times as bright as the next strongest airglow line, O I λ1304. As a result this line dominates a faint pseudo-continuum created by grating-scattered light in the spectrograph. The airglow subtraction is not expected to be exact because all of the airglow lines do not scale together. As a result, the "airglow-subtracted" spectrum still shows fairly strong emission from O I λ1304 and O I λ1356. The fluxed and airglow-subtracted spectrum, corrected for a reddening of $E(B-V) = 0.08$, is shown in Figure 2. As anticipated, the spectrum shows a number of emission lines from the SNR. In the 900–1200 Å range, the region inaccessible to *IUE*, these include S VI $\lambda\lambda$933, 945, C III λ977, and O VI $\lambda\lambda$1032, 1038. Longward of Lyα the strong lines include N V $\lambda\lambda$1239, 1243, O V λ1371, O IV] λ1400, C IV $\lambda\lambda$1548, 1551, and He II λ1640. A number of weaker features are also present and there is evidence of a faint continuum with a flux of $\sim 6 \times 10^{-15}$ ergs cm^{-2} s^{-1} $Å^{-1}$ at 1500 Å which may arise, at least in part, from hydrogen two-photon emission.

To characterize the data more quantitatively, we have fitted the sky-subtracted spectrum to a series of emission lines plus a two-photon continuum. The statistical errors of the HUT data are determined by Poisson counting statistics. As a result, it is straightforward to calculate the statistical error associated with the generation of the airglow-subtracted source spectrum. To fit the spectrum we have used a nonlinear χ^2 minimization IRAF routine, "specfit," developed by G. A. Kriss. For our global fit of the spectrum we have assumed that all multiplets have the relative strengths expected in the optically thin, low-density limit. We have also included a nonphysical power-law

[1] The cooling time $\tau = T^{3/2}n^{-1} \sim Pn^{-5/2}$ so the difference in cooling time can be considerable for a shock encountering a typical cloud with $n \sim 10$ cm^{-3} compared to a shock encountering neutral material with a density of order 0.1 cm^{-3}.

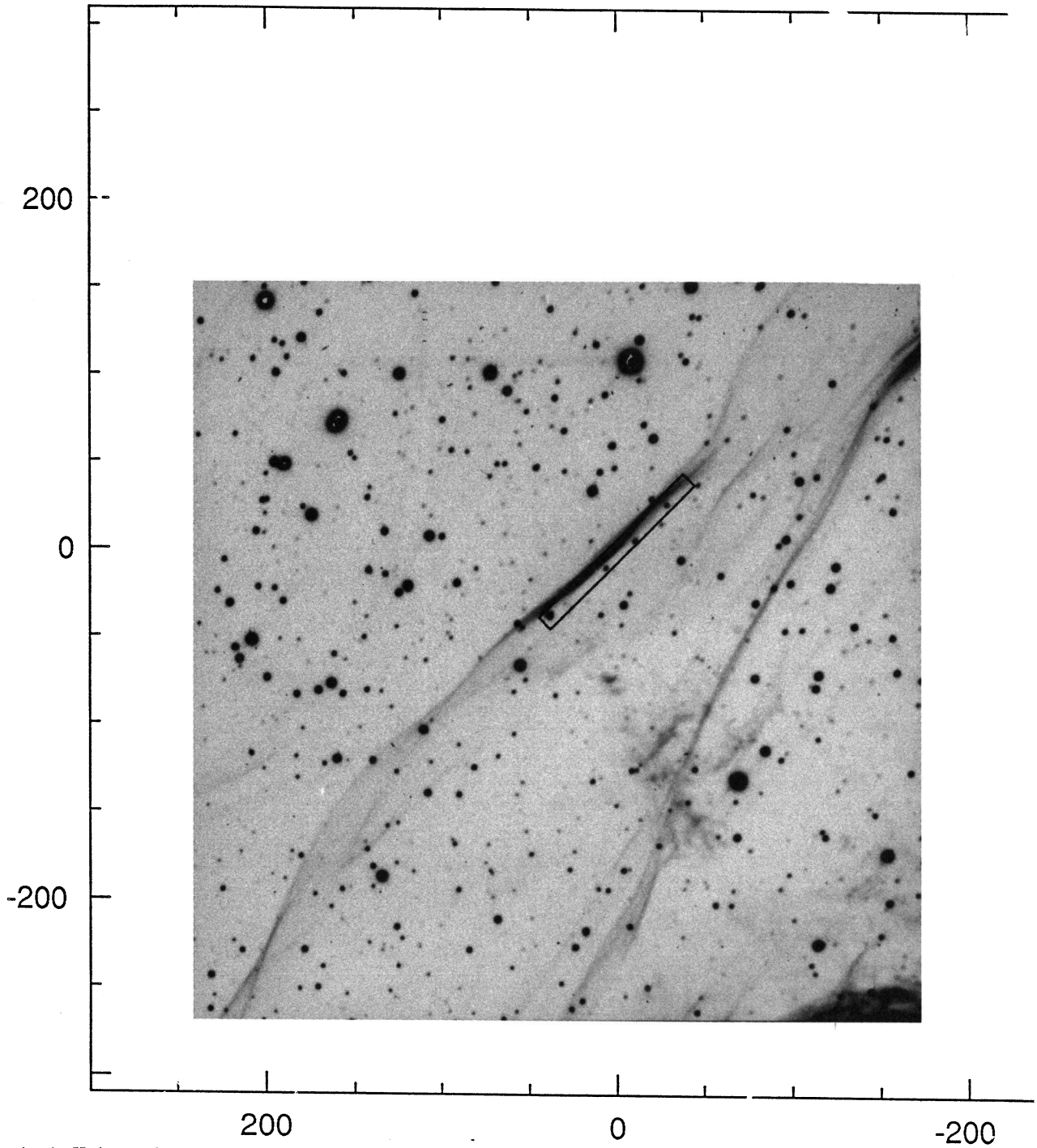

FIG. 1.—An Hα image of a position of northeastern limb of the Cygnus Loop. North is up, and east is to the left and the HUT aperture(9″.4 × 116″) is shown to scale.

LONG et al. (see 400, 215)

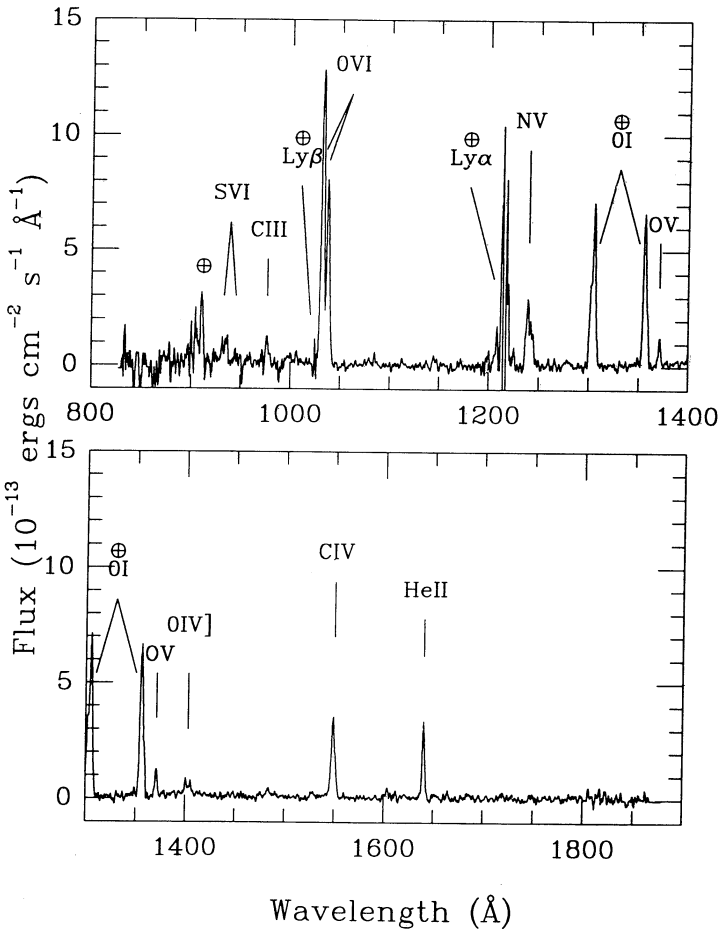

FIG. 2.—The HUT spectrum of the Balmer-dominated filament shown in Fig. 1. The spectrum has been flux-calibrated and airglow subtracted and corrected for an assumed reddening of $E(B-V)$ of 0.08. Residual airglow lines are indicated with an Earth symbol. The spectrum has been smoothed with a boxcar function with a width of 3 pixels (~1.7 Å).

component in the fits as a check on our dark count and sky subtraction. In the fit we have excluded regions below 920 Å, where there is a complex of poorly subtracted airglow features arising from O^+ recombination (Feldman et al. 1992), as well as a 20 Å region centered on Lyα and 10 Å regions centered on O I λ1304 and O I λ1356. The overall spectral fit has a χ^2 of 1940 for 1734 data points and 82 free parameters. (There are usually three free parameters, the exact line position, the line width, and the line center associated with each single line or multiplet.) The results are shown in Table 1. For converting observed to dereddened fluxes we have used $E(B-V) = 0.08$ and the mean galactic extinction curve derived by Seaton (1979), assuming it to be valid to 912 Å as indicated by Longo et al.'s (1989) analysis of *Voyager* observations. The errors on the line strengths represent 1 σ error bars. We have performed numerous checks of the strengths of individual lines over more limited regions and obtain the same results within the errors of the counting statistics.

Our global fit to the data indicates there is a two-photon continuum component to the observed spectrum, but it is very faint. The flux at 1520 Å, the peak of the two-photon spectrum, corresponds to 3.1×10^{-15} ergs cm^{-2} s^{-1} $Å^{-1}$. This corresponds to a total two-photon flux, integrated over all wavelengths, of 0.45 photons cm^{-2} s^{-1} or 3.8×10^{-12} ergs $cm^{-2}s^{-1}$. (As noted above, the apparent continuum flux is 1.6 times as large as the part we ascribe to the two-photon continuum; in the global fit the remainder went into the power-law component.) We have also fit the continuum portion of the data to models containing a two-photon continuum and the pseudo-continuum which would have resulted from an incorrect subtraction of the dark count rate. In that case we obtain a similar result: 3.2×10^{-15} ergs cm^{-2} s^{-1} $Å^{-1}$ for the two-photon component. HUT is a good instrument to study extended sources because of its large slit and large effective area. However, HUT is not the ideal instrument with which to search for an extremely faint, featureless continuum because it is not straightforward to determine the background with its one-dimensional detector. As a result, and despite the apparent agreement between the two model fits, we regard our determination of the two-photon flux as uncertain at the 50% level.

3. ANALYSIS AND DISCUSSION

RBFG observed just four lines—N V λ1240, Si IV + O IV] λ1400, C IV λ1549, and He II λ1640—in their *IUE* spectrum of the Balmer-dominated filament; our new observations have a much higher signal-to-noise ratio, but the ratios for these strong lines are about the same as seen with *IUE*. Additional fainter lines of carbon, oxygen, neon, and sulfur from the SNR as well as faint residual airglow features can also be seen in our HUT spectrum. The C IV flux we observe corresponds to a

TABLE 1

LINE FLUXES FOR A BALMER-DOMINATED FILAMENT IN THE CYGNUS LOOP

Ion	λ	$F(\lambda)$[a]	$I(\lambda)$[a]
S VI	933.4, 944.5	17.8 ± 3.6	28.3 ± 5.7
C III	977.0	12.4 ± 2.9	18.1 ± 4.3
N III	991.0	−3.0 ± 2.9	−4.3 ± 4.2
Ne VI	1006	5.8 ± 1.6	7.9 ± 2.2
O VI	1031.9, 1037.6	232.7 ± 8.0	299.6 ± 10.3
He II	1084.9	5.4 ± 1.7	6.4 ± 2.0
Ne V	1146	3.9 ± 1.4	4.3 ± 1.6
N V	1238.8, 1242.8	100.0 ± 7.8	100.0 ± 7.8
C II	1335.3	0.0 ± 1.1	0.0 ± 1.1
O V	1371.3	14.7 ± 2.2	13.7 ± 2.0
Si IV	1393.8, 1402.8	5.0 ± 2.4	4.6 ± 2.3
O IV]	1404[b]	16.8 ± 2.9	15.5 ± 2.7
N IV]	1486	7.0 ± 1.6	6.3 ± 1.4
C IV	1548.2, 1550.8	69.7 ± 4.5	62.6 ± 4.0
[Ne V]	1575	0.8 ± 1.0	0.7 ± 0.9
[Ne IV]	1602	5.3 ± 1.8	4.7 ± 1.6
He II	1640.5	47.1 ± 3.8	41.8 ± 3.4
O III]	1665	2.0 ± 1.2	1.8 ± 1.1
N III]	1750[b]	2.4 ± 2.4	2.0 ± 2.2
Two-photon[c]	All	306:	276:

[a] Scaled relative to N V = 100. The total flux F(N V) is 1.26×10^{-12} ergs cm^{-2} s^{-1}. The reddening-corrected flux I(N V) is 2.56×10^{-12} ergs cm^{-2} s^{-1}. The reddening correction was based on an $E(B-V)$ of 0.08 and the mean galactic extinction curve of Seaton (1979).

[b] Fit as a quintet of lines with relative line strengths fixed at those expected in the optically thin, low-density limit.

[c] The actual value of the two-photon continuum is somewhat uncertain. See text.

surface brightness of 6.3×10^{-5} ergs cm^{-2} s^{-1} sr^{-1}, about a factor of 2 below the value reported by RBFG with *IUE*; this is within the range of difference one might expect as a result of the differing *IUE* and HUT aperture sizes (see Fig. 1). RBFG concluded that their *IUE* spectrum could be interpreted in terms of a shock velocity of 170 km s^{-1} if the postshock electron and ion temperatures equilibrated on a Coulomb time scale, or 210 km s^{-1} if the temperatures equilibrated more rapidly. They favored Coulomb equilibration, and therefore we will use 170 km s^{-1} as a starting point for our interpretation of the HUT spectrum.

3.1. *Resonance Scattering*

The strongest lines in the HUT spectrum of the Balmer-dominated filament are the 1*s*–2*p* resonance doublets of O VI, N V, and C IV. Of the three doublets, only O VI is clearly separated at the 3.5 Å resolution of the HUT spectrograph. The O VI doublet ratio permits us to assess the optical depth of the O VI lines, and thereby to estimate the column density of the emitting gas and its density. This is also important because resonant scattering in a sheet of gas tends to reduce the intensities of resonance lines when the sheet is viewed edge-on, which is the case for the observed filament (see Fig. 1). Resonant scattering attenuates the C IV $\lambda\lambda$1548, 1551 intensities in some bright Cygnus Loop filaments by a factor of 3 (Raymond et al. 1988; Cornett et al. 1992). We have, therefore, performed a separate fit of the 50 Å region centered on O VI; in this fit the model components were Lyβ, O VI $\lambda\lambda$1032, 1038 and a power-law continuum. The best-fit model in which the O VI line ratios were allowed to vary yielded a χ^2 of 131.1 for 98 data points and nine free parameters; the ratio of λ1038:λ1032 was 0.60 ± 0.04. This should be compared to a best-fit value of χ^2 of 138.0 when the line ratio was fixed at 0.5, the value expected in the low-density, optically thin limit.

The measured O VI doublet ratio of 0.6 differs by 2.5 σ from the optically thin value. Since the oscillator strength of the 1038 Å line is a factor of 2 smaller than the 1032 Å line, the line ratio is related to the optical depth τ in the 1038 Å line as follows:

$$\frac{I_{\lambda 1038}}{I_{\lambda 1032}} = \frac{1 - e^{-\tau_{\lambda 1038}}}{1 - e^{-2\tau_{\lambda 1038}}} .$$

The ratio we observe, 0.60 ± 0.04, corresponds to optical depth $\tau_{\lambda 1038}$ between 0.24 and 0.58 with a best fit of 0.40. The probability that a photon with wavelength λ will escape is given by $(1 - e^{-\tau_\lambda})/\tau_\lambda$. This implies that the total observed O VI flux must be multiplied by a factor between 1.21 and 1.56. The correction for $\tau_{\lambda 1038} = 0.40$ is 1.37, and therefore we have used this correction to O VI for comparison with the models.[2] The C IV and N V column densities are several times smaller than that of O VI, so we expect no more than 10% attenuation of these lines. (As a result we have not applied a correction to these lines.)

The O VI optical depth is related to the O VI column density, but the relationship depends on the line width. Specifically,

$$\tau \sim N_{\rm O\ VI} \frac{\pi e^2}{mc} \frac{f}{\Delta v} ,$$

where $\Delta v = b v_0/c$ and f is the oscillator strength. Thermal broadening at 5×10^5 K (as expected from a shock velocity of 170 km s^{-1}) implies a Doppler parameter b of 23 km s^{-1}. Turbulence, or bulk velocity if the shock is slightly curved, might double this. For O VI λ1038, $f = 0.066$ (Morton 1991) and thus $0.24 < \tau_{\lambda 1038} < 0.58$ implies $6 \times 10^{13} < N_{\rm O\ VI} < 1.5 \times 10^{14}$ cm^{-2}. (Note: This estimate of the O VI column density would include any interstellar O VI which happens to lie along the line of sight to the Cygnus Loop, although values of O VI derived along the lines of sight to a number of nearby stars [Jenkins 1978] are an order of magnitude below the O VI columns derived here.) The surface brightness is given by

$$\frac{dI}{d\Omega}\,(\text{O VI}) = \frac{N_{\rm O\ VI} n_e q h\nu}{4\pi} ,$$

where the excitation rate q is 2.5×10^{-8} cm^3 s^{-1} at 5×10^5 K. (Note: here we have assumed that the emission fills the aperture uniformly. This is reasonable because the filament is 5″ wide in N V [RBFG] and probably wider in O VI.) The O VI surface brightness, corrected for reddening and resonance scattering is $\sim 3.3 \times 10^{-4}$ ergs cm^{-2} s^{-1} sr^{-1} and thus the inferred density behind the shock lies in the range 60–150 cm^{-3}. In strong shocks the postshock density is 4 times the preshock density, but the models discussed below have extensive enough cooling zones that a further factor of 3 compression occurs. As a result, the O VI doublet intensity and shape suggests a preshock density n_0 of 5–12 cm^{-3}.

Another approach to estimating the preshock density is to compare the flux observed with that predicted from shock

[2] The formulation described above is really only correct if τ_λ along the line of sight is much greater than τ_λ in the direction of the shock flow. In fact, the models described in the following section suggest O VI column densities and optical depths along the flow directions $\frac{1}{8}$ to $\frac{1}{4}$ as large as those along the line of sight. A two-dimensional radiative transfer calculation is needed. We expect that the observed doublet ratio corresponds to a slightly larger optical depth than we have derived, but that this should not have a large effect on the intensity correction factor.

models. The difficulty associated with this type of estimate is that the geometry of the shock front must be known. However, if we assume that we are viewing the nonradiative filament in the Cygnus Loop tangentially and that the emission is uniform along the slit, then the observed flux is given by

$$I_{\rm obs} \sim \frac{n_0}{n_{\rm mod}} \frac{dI_{\rm mod}}{d\Omega} \frac{d_{\rm slit}\, d}{D^2} = \frac{n_0}{n_{\rm mod}} \frac{dI_{\rm mod}}{d\Omega} \frac{\sin\,(116'')d}{D} ,$$

where $dI_{\rm mod}/d\Omega$ is the model prediction for the face-on surface brightness, D is the distance to the Cygnus Loop, 770 pc, $d_{\rm slit}$ is the length of the HUT slit at the distance of the Cygnus Loop, and d is the length of the filament along the line of sight. It is difficult to estimate d, but RBFG assumed 0.3 pc based on the apparent length of the filament on the sky. The 178 km s^{-1} model described below calculated for $n_0 = 1$ cm^{-3} yields face-on O VI and N V doublet surface brightnesses of 4.9 and 1.3×10^{-6} ergs cm^{-2} s^{-1} sr^{-1}. The dereddened and resonance-corrected fluxes we infer are 9.36×10^{-12} ergs cm^{-2} s^{-1} and 2.56×10^{-12} ergs cm^{-2} s^{-1}, which suggests values for n_0 of 8.7 and 9.0 cm^{-3}, respectively. Given the uncertainty in d, this is consistent with the estimates based on the doublet ratio and can perhaps be taken as an indication that the depth of the filament along the line of sight is indeed $\sim$0.3 pc. The preshock densities are somewhat higher than those inferred by RBFG and are comparable to those derived for the 130–140 km s^{-1} shock in the filament known as the Spur (Raymond et al. 1988).

3.2. *Model Comparisons*

In order to understand our observations in more detail we now compare our spectra to shock models using an updated version of the shock code described by Raymond (1979) and Cox & Raymond (1985). We use He II collision strengths based on Hayes (1987) and H collision strengths from Aggarwal (1983). The new shock code also allows much shorter time steps and unequal electron and ion temperatures. We assume either complete equilibrium of electron and ion temperatures due to plasma turbulence in the shock ($T_i = T_e$), or else ion-electron equilibration by Coulomb collisions alone in the postshock gas ($T_i \neq T_e$). In fact, most of the line intensities in the UV are not very sensitive to the degree of equilibration because the ions and electrons are fairly close to equilibrium by the time the ionization stage observed in the UV are achieved. The equilibration mostly affects the Hα line width expected for a given shock velocity (see RBFG and the discussion below).

RBFG assumed abundances for He, C, N, O, Ne, and Si (relative to H = 10,000) of 1000, 1.3, 0.62, 4.4, 0.8, and 0.11. These choices were based on typical diffuse cloud depletions and the assumption that the UV emission lines arise immediately behind the shock, before any significant grain destruction can occur, so that the depleted abundances are appropriate. We assume these abundances as well. We must also specify the sulfur abundance which we take to be 0.16 (Cowie & Songaila 1986).

An additional model parameter is the column density cutoff. Published shock models generally apply to "complete" radiative shocks, in which the shocked gas cools all the way to 1000 K (e.g., Hartigan, Raymond, & Hartmann 1987). The gas is too cool to emit in optical or UV light beyond that point, so the precise cutoff is unimportant. A fast nonradiative shock that ionizes the shocked gas beyond O VI also produces a UV spectrum independent of the cutoff, provided that the full O VI zone is present. The shock we are observing, however, does not produce high enough temperatures to ionize beyond O VI, so the O VI intensity continues to build up behind the shock until the gas cools and begins to recombine. Therefore, the accumulated column density (or equivalently the thickness of the shocked gas layer) is a necessary and important model parameter. Following the procedure outlined by Raymond et al. (1988), we plotted the accumulated intensities of various emission lines and chose a cutoff for the best match to the observations. The lower limit to the cutoff is determined largely by the ratio of high to intermediate ions (O VI to O IV and C IV), while the upper limit to the cutoff comes from the extremely rapid accumulation of lower ionization intercombination and forbidden lines (especially [O III] at optical wavelengths) once severe cooling sets in.

Table 2 compares various shock models with the HUT spectrum. All of the models are calculated assuming a preshock density of 2 cm^{-1}, a 30% preshock neutral fraction, and a column density cutoff of 10^{17} cm^{-2}. The neutral hydrogen fraction is important mainly for the intensities of the Balmer lines and two-photon continuum; we take it to be 0.3 (RBFG; Fesen & Itoh 1985). The first four models are calculated assuming instant equilibration of the electron and ion temperature behind the shock. The first three, calculated for velocities 175, 180, and 185 km s^{-1} show the sensitivity of the O VI $\lambda\lambda$1032, 1038:N V $\lambda\lambda$1239, 1243 ratio to the shock velocity. If the shock velocity were even 20 km s^{-1} greater, the O VI $\lambda\lambda$1032, 1038:N V $\lambda\lambda$1239, 1243 ratio would climb to 1000:100. It is clear that the "average" shock velocity must be fairly close to 180 km s^{-1} to match the O VI intensity. The fourth model, which has a shock velocity of 179 km s^{-1}, is the "best fitting" model with instant equilibration. It fits all of the lines well, except for C III λ977, which is not as strong in the model as observed. As we indicated earlier, the UV line strengths, especially the strengths of the dominant high-ionization lines, are not very dependent on the assumptions made about the rate of electron-ion equilibration. The largest differences in the UV are in the low-ionization lines, which are stronger for Coulomb equilibration than for instant equilibration. The fifth model shown in Table 1, is the "best-fitting" model assuming that electrons and ions equilibrate on a Coulomb time scale ($T_i \neq T_e$). It is also in good agreement with the data; it also fits C III λ977 accurately.

RBFG could not determine the shock velocity on the basis of the UV spectra alone because there are no lines in the *IUE* range which have "turn-on" velocities greater than $\sim$150 km s^{-1}. Instead, they based their determination of the shock velocity on the width of Hα. In nonradiative shocks, Balmer photons are emitted as neutral hydrogen atoms pass through the shock front (CKR). A narrow Hα line is observed from those neutrals which are excited before being ionized in the postshock gas. A broad component is observed from a population of fast neutrals behind the shock which are created because the charge transfer cross section between slow neutrals entering the shock and fast protons behind the shock is large. Both the Doppler width of the broad component and the ratio of broad to narrow line emission are measures of the postshock proton temperature.

The exact relationship between the shock velocity and the width of the broad component depends on the rate of equilibration of the electron and ion temperatures behind the shock. RBFG used an echelle spectrum obtained with the 60″ (1.5 m) telescope at Mount Hopkins Observatory to measure the

TABLE 2

COMPARISON OF RELATIVE FLUXES WITH MODELS

LINE		OBSERVED	MODELS[a]					
Ion	λ_{vac}	$I(\lambda)$	I175	I180	I185	I179	C184	SUM[b]
S VI	933.4, 944.5	28.3 ± 5.7	27.8	27.5	26.8	27.3	28.6	31.4
C III	977.0	18.1 ± 4.3	6.8	6.8	6.9	6.6	17.3	47.2
N III[c]	991.0	−4.3 ± 4.2	0.8	0.8	0.8	0.7	1.8	5.1
O VI[d]	1031.9, 1037.6	365.5 ± 12.5	229.0	433.0	586.0	413.0	389.0	375.0
He II	1084.9	6.4 ± 2.0	9.7	10.7	11.8	11.5	11.5	23.5
N V	1238.8, 1242.8	100.0 ± 7.8	100.0	100.0	100.0	100.0	100.0	100.0
O V	1371.	13.7 ± 2.0	11.1	11.5	11.8	11.5	11.5	11.0
Si IV	1393.8, 1402.8	4.6 ± 2.3	1.7	1.7	1.6	1.7	2.9	7.4
O IV	1404[b]	15.5 ± 2.7	15.1	11.5	9.4	12.0	14.6	33.3
N IV]	1486	6.3 ± 1.4	2.6	2.0	2.0	2.1	2.7	6.9
C IV	1548.2, 1550.8	62.6 ± 4.0	63.8	60.0	58.5	59.0	73.1	162.0
[Ne IV]	1602	4.7 ± 1.6	0.7	0.5	0.4	0.5	0.6	1.6
He II	1640.5	41.8 ± 3.4	40.6	44.6	49.5	43.0	52.6	98.5
O III]	1665	1.8 ± 1.1	0.5	0.5	0.4	0.5	1.3	5.6
N III	1750[b]	2.0 ± 2.2	0.1	0.1	0.1	0.1	0.3	1.2
Two-photon	...	276:	227.0	256.0	259.0	220.0	362.0	855.0

[a] Models labeled I were calculated assuming instant equilibration ($T_i = T_e$). Models labeled C were calculated using coulomb equilibration ($T_i \neq T_e$). The number associated with each model is the velocity in km s^{-1}.

[b] See text for description of model for a decelerating shock. Coulomb equilibration was assumed in constructing this shock.

[c] There was an airglow line at this position in the on-source data. The limit we derive on the strength of N III is somewhat uncertain due to this fact.

[d] O VI has been corrected for resonance scattering. See text.

width of the broad component of Hα to be 167 km s^{-1} (FWHM). From this value, RBFG inferred that the shock velocity was near 170 km s^{-1} for Coulomb equilibration and 210 km s^{-1} for instant equilibration (Note: The neutrals behind the shock are ionized quite rapidly. For a given shock velocity, instant equilibration results in a lower ion temperature in the "neutral zone" because the postshock energy is shared quickly among electrons and ions.) On the basis of these arguments, our observation with HUT would seem to provide strong confirmation for equilibration on a Coulomb timescale.

However, Hester, Raymond, & Blair (1992) have obtained higher quality echelle spectra of this filament with the KPNO 4.0 m telescope and a CCD detector. Their spectra have better spectral resolution and much higher signal to noise than those of RBFG, and they measure 135 ± 5 km s^{-1} (FWHM) for the broad component. This suggests a shock velocity for the nonradiative filament observed with HUT of 135 km s^{-1} for Coulomb equilibration or 170 km s^{-1} for instant equilibration. Furthermore, the ratio of broad to narrow line emission measured by Hester et al. (1992), 1.68, is constant with ratio of 1.65 predicted by Smith, Laming, & Raymond (1992) for a fully equilibrated 175–180 km s^{-1} shock, and inconsistent with the ratio of 2.81 predicted for a 135 km s^{-1} shock with Coulomb equilibration.

Since the HUT data imply an "average" shock velocity of ~180 km s^{-1}, the simplest interpretation of both the HUT spectrum and the Hα line width is that we are looking at a fully equilibrated 175–180 km s^{-1} shock. There are some difficulties, however, with this appealing interpretation: (1) Optical spectra of this nonradiative filament show more [O III], [S II], and [N II] than would be produced in this simple picture (RBFG; Fesen & Itoh 1985). The [O III]:Hα intensity ratio, which Fesen & Itoh measure to be 0.05, is predicted to be less than 0.02 in the 175–180 km s^{-1} models assuming instant equilibration. The HUT spectrum also contains more emission from some lines, most notably C III λ977, than predicted in the fully equilibrated models. (2) Comparison of model calculations with observations of Tycho's SNR, SN1006, and other high velocity nonradiative shocks provides fairly strong evidence against full equilibration models at 1000–2000 km s^{-1} (Smith et al. 1992). (3) There is no theoretical basis for instant equilibration. Indeed, theoretical calculations (Cargill & Papadopoulos 1988) suggest that equilibration immediately behind the shock is modest ($T_e \sim 0.22 T_i$).

An obvious possibility that avoids these problems is to assume that the shock is slowing down, either because it is entering denser material (e.g., McKee et al. 1987) or because thermally unstable cooling is taking place behind the shock allowing it to decelerate[3] (Chevalier & Imamura 1982; Innes, Giddings, & Falle 1987; Gaetz, Edgar, & Chevalier 1988). This possibility is appealing because the Balmer line emission must arise within 10^{15} cm of the shock front while the zones which generate the higher ionization lines lie at least 10^{16} cm from the shock front. It is likely that the shock is entering a denser medium because the time for a 180 km s^{-1} shock encountering an ISM density of 2 cm^{-3} to develop a partial recombination zone is short—200 yr—in which time it would have traversed only 10^{17} cm or 10″ on the sky. If this shock has been traversing gas with this density for much greater than 200 yr, one would expect to see much stronger emission from lower ionization lines, such as [O III] and [S II], which are characteristic of radiative shocks.

[3] Innes (1992) has recently calculated spectra for thermally unstable radiative shocks with a velocity of 175 km s^{-1}. These model spectra have much stronger emission from low-ionization transitions in the UV and in the optical than is observed in the Balmer-dominated filament being discussed here. Nevertheless, the thermal instability that Innes (1992) describes, which should be operative at this shock velocity, could contribute to the deceleration of the shock front. The spectra calculated by Innes (1992) are likely to be much more relevant to the other filament observed with HUT in the Cygnus Loop discussed briefly in § 3.3. (See also Blair et al. 1991a.)

In the absence of published models for decelerating shock waves with relevant shock parameters, we have constructed a rough model by simply adding the emission from steady flow shock models of 130, 140, ..., 200 km s^{-1} with Coulomb equilibration, taking the emission from the first 1.25×10^{16} cm^{-2} of hydrogen column density from the 130 km s^{-1} model, the emission from the 1.25×10^{16}–2.5×10^{16} cm^{-2} zone of the 140 km s^{-1} model, and so on up to 1.0×10^{17} cm^{-2}. This "summed" model is shown in the last column of Table 2. The "summed" model reproduces the O VI to N V ratio which is observed, and it results in Balmer lines with the appropriate broad component. Several other lines, S VI and O V, also fit well, but, overall, the summed model does not fit the data as well as the single velocity, steady flow models discussed earlier. Specifically, the summed model produces two-photon, He II, C III, C IV, O III, and O IV emissions 2–4 times stronger than observed. While the "summed" model is a rather crude approximation for a rapidly decelerating shock, its poor agreement with the observations strongly suggests that fairly complete electron-ion equilibration in the shock is more likely. It is possible to get around any one of these problems by, for instance, reducing the hydrogen neutral fraction or assuming a stronger depletion of carbon, but such changes would be likely to cause difficulties with other line ratios. Thus we conclude that the HUT spectrum favors at least partial electron-ion equilibration. If $T_e = 0.5T_i$ at the shock, the observed Hα width corresponds to $v_s = 147$ km s^{-1}. That would bring the discrepancies between model and observation to about the same level as the discrepancy between the equilibrated model and observation.

3.3. *Comparison with the Incomplete Shock Observed with HUT*

As the nonradiative shock in the NE evolves it will eventually begin to develop a recombination zone. At optical wavelengths the first indication that a recombination zone is developing will be a dramatic increase in the flux in [O III], which becomes an important coolant as soon as the postshock gas cools to ~50,000 K. In the most common shocks, shocks that have fully developed recombination zones, [O III]:Hβ ratios ranging from 1:1 to 3:1 are typical. There are other shocks, however, in the Cygnus Loop and elsewhere that have [O III]:Hβ ratios as high as 40 (Fesen, Blair, & Kirshner 1982). These are usually called "incomplete shocks" because the forbidden lines, such as [O I], [N II], and [S II], which are expected when the postshock gas cools to 10,000–20,000 K, are weak.

The other Cygnus Loop filament observed with HUT (Blair et al. 1991a) is an incomplete shock on the eastern limb. Although the encounter of this shock with a cloud probably predates that of the nonradiative shock in the north, it is likely that the shock conditions were rather similar. In fact, the high-ionization lines—O VI λλ1032, 1038, N V λλ1239, 1243, C IV λλ1548, 1551 and He II λ1640—have similar line ratios at the two positions and as a result, Blair et al. (1991a) conclude that a shock velocity of 167 km s^{-1} is required to account for the UV emission of the dominant ions. The principal difference between the HUT spectra at the two positions is that the lower ionization lines are more prominent in the "incomplete" shock. For example, the ratios of O VI λλ1032, 1038:O V λ1371:O IV] λ1400:O III] λ1663 in the nonradiative filament are 1.0:0.05:0.04: <0.01, while the corresponding ratios for the incomplete radiative shock are 1.0:0.13:0.87:0.66. Blair et al. (1991a) suggest that the lower ionization lines arise in lower velocity shocks; these may be either physically different shocks seen along the same line of sight as the 170 km s^{-1} shock or a single shock which has undergone the thermal instability discussed by Innes et al. (1987), Gaetz et al. (1988), and Innes (1992). Thus, the nonradiative shock seems to have a similar shock velocity, but a less complete cooling zone, or a smaller admixture of low-velocity shocks, than the incomplete radiative filament observed with HUT. The lower velocity shocks would arise naturally in the picture of the decelerating shock described above as the shock penetrates further into the denser core of a cloud. Thus it seems quite likely that within a few hundred years the northern limb of the Cygnus Loop will look much more like the rest of the Cygnus Loop than it does today.

3.4. *Comparison with* Voyager *Results*

The two *Voyager* spacecraft carried Ultraviolet Spectrometers (UVSs) as part of their instrumentation for investigating planetary atomospheres. During interplanetary cruise periods, the UVSs have been used to obtain FUV (500–1700 Å) observations of many astronomical sources, including the Cygnus Loop (Shemansky, Snadel, & Broadfoot 1979). For extended sources, the *Voyager* resolution is ~38 Å, significantly worse than *IUE* or HUT, but the large 0°.1 × 0°.87 field of view (FOV) of the UVSs allowed Blair et al. (1991b) to produce a crude map of the 900–1200 Å emission from the entire Cygnus Loop. There are two prominent peaks at 980 and 1035 Å in the sub-Lyα *Voyager* spectra. The luminosity in these lines exceeds that of the Cygnus Loop at X-ray wavelengths. Blair et al. (1991b) argue that the peaks are most likely due to C III λ977 and O VI λλ1032, 1038. The HUT data (Blair et al. 1991a and this paper) basically confirm their line identifications. (At the other shock position, N III λ991 is also fairly strong and so it may contribute to the 980 Å peak at some positions.) Blair et al. (1991b) show that substantial spatial variations are present in the absolute and relative intensity of these lines. However, blending of many different filaments in the large *Voyager* FOV made it unclear whether O VI emission came mainly from the bright optical filaments, the primary shock front, or (more probably) both. This blending also made it difficult to assess the real range of variations in the O VI:C III ratio for individual filaments.

The HUT spectrum here, of the nonradiative filament near the primary shock in the Cygnus Loop, shows clearly that the blending of emission in the *Voyager* FOV causes the peak of the O VI:C III ratio to be severely underestimated. From Table 2, this ratio is seen to be ~20, as compared to a peak ratio of ~3 for the *Voyager* data (Blair et al. 1991b). Similarly, it seems almost certain that there are filaments with O VI:C III ratios of less than the minimum value of 0.6 which Blair et al. (1991b) reported.

The data at the two HUT positions confirm that O VI emission is coming both from regions of bright optical emission and from Balmer-dominated filaments near the primary (X-ray) shock front. This makes sense in the context of the picture presented in § 3.3 in which the filaments observed at the two HUT positions represent the same phenomenon at slightly different epochs after the shock/cloud encounter.

4. SUMMARY

We have used the Hopkins Ultraviolet Telescope to observe the brightest nonradiative filament in the Cygnus Loop. The spectrum is of much higher signal to noise than the corre-

sponding spectrum obtained with *IUE*. Our spectrum extends to the Lyman limit and includes O VI $\lambda\lambda$1032, 1038, so we are able to determine the shock velocity of the filament to be 175–185 km s^{-1} directly from UV line strengths. This shock velocity can be reconciled with the most recent measurements of the width of the broad component of Hα of 135 km s^{-1}, but only if instant equilibration of electrons and ions in the postshock gas is assumed.

The fact that the filament is visible but does not have a large recombination zone implies that the shock has encountered a density enhancement fairly recently. If the density is continuing to increase, or if the shock is decelerating for other reasons, it may ultimately be possible to reconcile the UV line strengths and the Hα line width with Coulomb equilibration. Detailed calculations are needed, however, because the simple modeling we have performed of a decelerating shock fails to match the UV spectrum.

It is not possible to acknowledge all of the engineers and scientists at Johns Hopkins and at NASA who contributed to the success of HUT and *Astro-1*. Here we would like to thank especially the mission managers from NASA/MSFC: Leon B. Allen, who oversaw the construction and delivery of HUT and the other instruments to KSC, and Jack Jones, who directed *Astro* from the period following the Challenger disaster through its launch in late 1990. The HUT project was funded by NASA contract NAS 5-27000 to The Johns Hopkins University. J. C. R. acknowledges NASA grants NAG5-87 and NAGW-528 to the Smithsonian Astrophysical Observatory.

REFERENCES

Aggarwal, K. M. 1983, MNRAS, 202, 15P
Benvenuti, P., Dopita, M., & D'Odorico, S. 1980, ApJ, 238, 613
Blair, W. P., Long, K. S., & Vancura, O. 1991, ApJ, 366, 484
Blair, W. P., et al. 1991a, ApJ, 379, L33
Blair, W. P., Long, K. S., Vancura, O., & Holberg, J. B. 1991b, ApJ, 374, 202
Braun, R., & Strom, R. G. 1986, A&A, 164, 208
Cargill, P. J., & Papadopoulos, K. 1988, ApJ, 329, L29
Chevalier, R. A., & Imamura, J. N. 1982, ApJ, 261, 543
Chevalier, R. A., Kirshner, R. P., & Raymond, J. C. 1980, ApJ, 235, 186 (CKR)
Chevalier, R. A., & Raymond, J. C. 1978, ApJ, 225, L27
Cornett, R. H., et al. 1992, ApJ, 395, L9
Cowie, L. L., & Songaila, A. 1986, ARA&A, 24, 499
Cox, D. P., & Raymond, J. C. 1985, ApJ, 298, 651
Davidsen, A. F., et al. 1992, ApJ, 392, 264
Feldman, P. D., et al. 1992, Geophys. Res. Lett., 19, 453
Fesen, R. A., Becker, R. H., Blair, W. P., & Long, K. S. 1989, ApJ, 338, L13
Fesen, R. A., Blair, W. P., & Kirshner, R. P. 1982, ApJ, 262, 171
Fesen, R. A., & Itoh, H. 1985, ApJ, 295, 43
Gaetz, T. J., Edgar, R. J., & Chevalier, R. A. 1988, ApJ, 329, 927
Hartigan, P., Raymond, J., & Hartmann, L. 1987, ApJ, 316, 323
Hayes, M. A. 1987, in Proc. Atomic Data Workshop Assessment of Data for Photoionization and for Electron Impact Excitation of Atomic Ions, ed. W. Eissner & A. E. Kingston (Daresbury: Daresbury Laboratory), 120
Hester, J. J., Raymond, J. C., & Danielson, G. A. 1986, ApJ, 303, L17
Hester, J. J., Raymond, J. C., & Blair, W. P. 1992, in preparation
Innes, D. E. 1992, A&A, 256, 660
Innes, D. E., Giddings, J. E., & Falle, S. A. E. G. 1987, MNRAS, 226, 67
Jenkins, E. B. 1978, ApJ, 220, 107
Keen, N. J., Wilson, W. E., Haslam, C. G. T., Graham, D. A., & Thommasson, P. 1973, A&A, 28, 197
Kirshner, R. P., & Chevalier, R. A. 1978, A&A, 67, 267
Kirshner, R. P., Winkler, P. F., & Chevalier, R. A. 1987, ApJ, 315, L35
Ku, W. H.-M., Kahn, M., Pisarski, R., & Long, K. S. 1984, ApJ, 278, 615
Long, K. S., & Blair, W. P. 1990, ApJ, 358, L13
Long, K. S., Blair, W. P., & van den Bergh, S. 1988, ApJ, 333, 749
Longo, R., Stalio, R., Polidan, R. S., & Rossi, L. 1988, ApJ, 339, 478
McKee, C. F., & Hollenbach, D. J. 1980, ARAA, 18, 219
McKee, C. F., Hollenbach, D. J., Seab, C. G., & Tielens, A. G. G. M. 1987, ApJ, 318, 674
Miller, J. M. 1974, ApJ, 189, 239
Morton, D. C. 1991, ApJS, 77, 119,
Raymond, J. C. 1979, ApJS, 39, 1
Raymond, J. C., Black, J. H., Dupree, A. K., Hartmann, L., & Wolff, R. S. 1980, ApJ, 238, 881
———. 1981, ApJ, 246, 100
Raymond, J. C., Blair, W. P., Fesen, R. A., & Gull, T. R. 1983, ApJ, 275, 636 (RBFG)
Raymond, J. C., Hester, J. J., Cox, D., Blair, W. P., Fesen, R. A., & Gull, T. R. 1988, ApJ, 324, 869
Schweizer, F., & Lasker, B. M. 1978, ApJ, 226, 167
Seaton, M. J. 1979, MNRAS, 187, 73P
Shemansky, D. E., Sandel, B. R., & Broadfoot, A. L. 1979, ApJ, 231, 35
Smith, R. C., Kirshner, R. P., Blair, W. P., & Winkler, P. F. 1991, ApJ, 375, 652
Smith, R. C., Laming, M. L., & Raymond, J. C. 1992, in preparation
Tuohy, I. R., Dopita, M. A., Mathewson, D. S., Long, K. S., & Helfand, D. J. 1982, ApJ, 261, 473